



OPEN Predicting cardiac frequencies in mammals

Rui D. M. Travasso¹, Clint A. Penick², Robert R. Dunn³ & E. Corvera Poiré^{4,5}✉

We develop a fluid mechanical model of the arterial tree in order to address the key question of what determines heart rate in mammals. We propose that the frequency of the pulsatile pressure gradient, which minimizes resistance to flow and facilitates fluid movement, coincides with the physiological heart rate. Using data from the literature on heart rate in 95 mammals as a function of body mass, and the radius of the aorta as a function of body mass, we construct a target curve of cardiac frequency versus aortic radius. This curve serves as a benchmark for comparison with our model's results. Our elastic one-dimensional model for pulsatile arterial flow, combined with experimental rheological data for human blood, enables us to calculate the frequency that minimizes flow resistance, which we express as a function of a characteristic vascular scale, in this case, the aorta radius. We find a reasonable agreement with the target curve, confirming a scaling law with the observed exponent for mammals ranging in size from ferrets to elephants. Our model provides a plausible explanation for the resting heart rate frequency in healthy mammals.

The daily functioning of mammal bodies involves many repetitive processes that require the movement of fluids from breathing to coughing or blinking. Among these, the beating of the heart is perhaps the most fundamental one. The rate of such repetitive processes, including the heart rate, tends to be characteristic of each individual species. Scaling laws have been proposed for the number of capillaries, blood volume, or circulation time as a function of the body mass of the species¹. However, the explanation for heart rate frequency has remained elusive. While the classical paper of West¹ proposed a scaling relation of $\nu \sim W^{-0.25}$, as the dependence for the heart rate, ν , on the body mass, W , observed data from mammals suggest the different scaling $\nu \sim W^{-0.16}$ (see below). Therefore, the important question remains: why do mammal hearts beat at the rates they do? Understanding this is crucial for understanding the evolutionary biology of cardiovascular systems. A model intending to explain heart rates should be grounded in an understanding of the factors that govern the evolution of heart rate, including those that derive from biophysical constraints. The aim of this paper is to give a plausible mechanical explanation of the physical factors driving the evolution of mammalian heart rates.

Over a decade ago, a simple model was proposed to explain resting heart rates in mammals, i.e., the number of heart beats per unit time when the organism is at rest². In that study (in which one of us was a coauthor) it was concluded that natural selection did not optimize heart rates for the efficient transport of blood through the entire vascular network. Instead, resting heart rates appeared to be optimized for blood flow in large arteries. Like when pushing oneself on a swing, some periodicities of blood pumping through the arteries enhance the blood flow, and others reduce it. At the time, the study assumed a Maxwell model for blood -one of the simplest models accounting for viscoelasticity, that considers a single relaxation time³-, flowing through a rigid network of vessels. However, with new insights into the nature of physiological frequencies and the availability of a large database on heart rates among mammals (see Supplementary Material), we are now able to reanalyze the problem with a more accurate model that incorporates: vessel elasticity, which better captures physiological behavior, accounting for pulse wave propagation, energy storage, and damping and is critical for realistic modeling of blood flow dynamics; a better description of the geometrical features of large and small arteries; as well as experimental information of human blood rheology, that provides accurate, material-specific data capturing the true viscoelastic behavior across a wide range of frequencies and avoids the oversimplifications of a Maxwell model that potentially misses key features, like multiple relaxation times. In short, this study investigates the pulsating frequency that minimizes resistance to flow in the elastic arterial tree. Our hypothesis is that this one will coincide with the heart rate in healthy mammals.

Fluid response to pulsatile pressure gradients, such as those associated with coughing or the pumping of a heart, have been described for simple geometries by the theory of the dynamic permeability. The dynamic

¹FisUC, Department of Physics, University of Coimbra, Rua Larga, 3004-516 Coimbra, Portugal. ²Department of Entomology and Plant Pathology, Auburn University, Auburn, AL 36849, USA. ³NC State University, 201B Holladay Hall, CB 7101, Raleigh, NC 27695, USA. ⁴Departamento de Física y Química Teórica, Facultad de Química, Universidad Nacional Autónoma de México, 04510 Mexico City, Mexico. ⁵UBICS Institute of Complex Systems, Universitat de Barcelona, Martí i Franquès 1, 08028 Barcelona, Spain. ✉email: eugenia.corvera@gmail.com

permeability is proportional to the ratio between the flow along the network and the pressure drop in the frequency domain. The equation that describes this relationship has been obtained theoretically for numerous systems: Newtonian, Maxwellian and general linear viscoelastic fluids in a wide range of rigid confining geometries^{4–12}; for two coexisting fluids -one viscous and one viscoelastic- flowing parallel to each other in a rigid tube¹³; and for Newtonian and viscoelastic fluids confined in elastomeric materials^{14–16}. Numerically, it has been obtained for compressible binary fluids¹⁷ flowing in series -one after the other one. All these studies show that when a system contains elastic elements, whether in the fluid (e.g., blood, mucus or polymers), in the confining media (e.g., vessels or PDMS microchannels), or in both, resonances emerge in the dynamic permeability that indicate the particular pulsatile frequencies of the pressure gradient that could maximize the amplitude of fluid velocity and minimize the resistance to flow.

The experimental observation of resonance consists of the observation of an increase in flow velocity amplitude at a specific frequency or range of frequencies of the driving pressure gradient. For single fluids, resonances were first reported experimentally at macroscales almost two decades ago^{18,19}. In these works the authors observe the oscillatory dynamics of Newtonian and Maxwellian fluids. For the latter ones the fluid flow velocity amplitude increases at specific oscillation frequencies. Recently, the pulsatile dynamics of a fluid slug consisting of a Newtonian²⁰ or a polymeric viscoelastic fluid²¹ and two air-fluid interfaces (which introduce elastic elements in the system) in a rectangular microchannel, was studied theoretically and validated experimentally by means of imposing a pulsatile pressure gradient through a piezoelectric device. The dynamic permeability of both Newtonian and viscoelastic systems presented resonances with excellent agreement between theory and experiment in the linear regime. The experimental results have validated the use of the dynamic permeability as a theoretical tool to study fluid responses to pulsatile pressure gradients.

A few years ago, an in-house Generalized Darcy's Elastic Model (GDEM) was developed and validated (by comparing flow and pressure waveforms with results of a fully non-linear 3-dimensional model) to describe the human arterial system²². This model was then used to study the cooperation between elasticity and bifurcations in symmetric tree-like networks, such as those found in the arterial system¹⁵. In the latter publication, we were able to relate linearly the velocity of the fluid and the pressure gradient in frequency domain for symmetric tree-like networks through a dynamic response function. This dynamic response function for networks, which is the ratio of the average flow along the flow direction and the pressure drop in the frequency domain, has the same properties that the dynamic permeability does for simpler geometries (like a single cylinder or a rectangular channel), namely, it presents resonances whenever there are elastic elements in the system. In the case of the arterial tree, both vessels and blood introduce in the system a certain degree of elasticity.

From these previous works we observe that fluid viscoelasticity, vessel elasticity and network branching morphology all can lead to the presence of resonance peaks in the dynamic permeability. For this reason, to study the maxima in the response function of arterial trees, we need a model that incorporates these three aspects.

Here, we study the pulsatile flow of blood confined in a tree-like arterial network whose bifurcating structure follows different rules depending on whether the bifurcating vessel is a large or a small artery. Large arteries bifurcate according to an area preserving law and small arteries according to Murray's law for radii¹. The two regions of the network have lengths that also follow different exponents depending on whether they are large or small arteries, where large and small refer to the radii rather than lengths. For large human arteries, we use the relationship between the lengths and the radii of vessels as measured from a 55-vessel model of the arterial system that describes with good accuracy the human arterial tree²³. Notably, in the large arteries region of the tree, length *increases* as radius *decreases*, reflecting the characteristics illustrated properly by the cases of the ascending aorta (with large radius and small length) and the iliac arteries (with small radii and large lengths). On the other hand, for small arteries (such as arterioles and capillaries), a space filling hypothesis¹ together with Murray's law for radii, dictate that length *increases* linearly as radius *increases*. In other words, while narrower large arteries tend to be longer arteries, narrower arterioles and capillaries tend to be shorter arterioles and capillaries. For species other than humans, we assume that the number of levels for small arteries is constant across species such that the curve of length as a function of radius does not depend on body mass¹. That is, for small arteries, the linear relationship between length and radius is preserved across species.

Finally, we use published data in the literature for seven species of mammals, from mice to horses, to propose a relationship between the length and radius of the aorta. These ones, follow a scaling law given by $l_{aorta} \sim r_{aorta}^{0.89}$ ²⁴. Continuity of the curve length vs radius determines the crossover level between large and small arteries and determines the power law behavior for large arteries, for each of the species.

With these considerations, we find that the frequency that maximizes the dynamic response function decreases as a power law of the radius of the widest vessel in the system (the aorta). This allows us to propose a plausible explanation for the heart rate, as the one which minimizes the resistance to flow (maximizes the network response) across the network, such that species with wider aortas will tend to have lower heart rates.

Methods

Actual Heart rate in mammals

Since allometric relations for mammal features have normally been given as a function of body mass¹, we report here documented heart rates vs mass for 95 mammal species. We were able to do so thanks to the work of citizen scientists who have combed the scholarly literature on heart rates over 60 years (see Supplementary Material). The mammals included in this dataset span a body size ranging from 1 kg to 3800 kg and cover several hundred million years of mammalian evolution. It is noteworthy that the most comprehensive comparison of heart rates among mammals before this one included just 16 species²⁵. The observational data from this database (see Supplementary Material) are depicted in Fig. 1. The continuous line is the best fit to a power law, given by

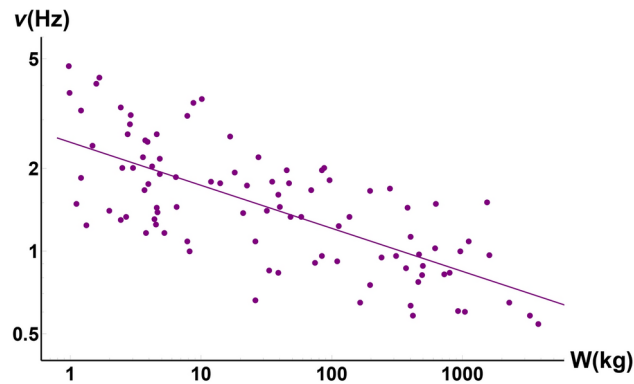


Fig. 1. Heart rates vs body mass for 95 mammals. Continuous line: fit to the observed data, $\nu = 2.49 W^{-0.16}$. Numerical values of data points are listed in Supplementary Material.

$\nu = 2.49 W^{-0.16}$ with ν expressed in Hz and W in kg. The fit was done with a simple linear regression of the logarithm of frequency data and the logarithm of body weight data.

On the other hand, models for the arterial system are able to characterize flow features as a function of some key dimension of the cardiovascular system, particularly the radius of the aorta. In order to take into account aorta size for hearts of diverse mammals, we have taken a scaling exponent for the aorta radius as a function of body mass from the literature, $r_{aorta} = 0.21 W^{0.36}$, with r_{aorta} expressed in cm and W in kg. This equation is based on the study of aorta diameter among seven species of mammals ranging from mice to horses²⁴. The above mentioned scaling relation of aorta radius with mass was used together with data of heart rates as a function of body mass (Fig. 1), to obtain a curve of heart rate as a function of aorta radius, $\nu = 1.25 r_{aorta}^{-0.43}$. The fit was done with a simple linear regression of the logarithm of frequency data and the logarithm of aorta radius data. This curve will be the reference curve we use to validate our model results.

Flow through a single elastic vessel

We describe the problem using continuum mechanics, because it effectively models both the fluid dynamics of blood flow and the mechanical behavior of the arterial walls. This approach accounts for the continuous and deformable nature of both blood and vessels, and it can handle the complex geometries, pulsatile flow, and dynamic interactions within the arterial system. In this section, we present what can be considered as the building block of our model, which is the model for blood flow through a single elastic vessel.

Darcy's model gives a linear relation between flow, \hat{q} , and pressure gradient, $\frac{\partial \hat{p}}{\partial z}$, in frequency domain. Hats over quantities denote Fourier transforms of quantities in time domain. We have derived the equations for a single rigid vessel containing blood in the Supplementary Material. In order to generalize such Darcy's model to elastic cylindrical vessels, we assume that it is valid locally, that is, at any point z along the flow direction of a vessel of average cross-section area A , that is,

$$\hat{q}(z) = -AK(\omega) \frac{\partial \hat{p}}{\partial z}(z), \quad (1)$$

where

$$K(\omega) = -\frac{1}{i\omega\rho} \left[1 - \frac{2J_1(\beta r)}{\beta r J_0(\beta r)} \right] \quad (2)$$

is the dynamic permeability of the fluid, which is a measurement of the resistance to flow; J_0 and J_1 are Bessel functions of the first kind of orders 0 and 1 respectively, ρ is the fluid density, the argument β is given by $\beta^2 = \frac{i\rho\omega}{\hat{g}(\omega)}$, r is the average radius of the elastic vessel, and $i = \sqrt{-1}$. The quantity $\hat{g}(\omega)$ is the relaxation modulus of the fluid in frequency domain; it is related to the stress tensor governing the fluid and can be determined experimentally. Flow is approximated as a velocity averaged over the average cross sectional area, A , times this area.

A second equation is given by the linear relationship between pressure and flow gradient, coming from mass conservation and a Hooke-like linear model for vessel elasticity²², namely

$$\hat{p}(z) = \frac{1}{i\omega C} \frac{\partial \hat{q}}{\partial z}(z), \quad (3)$$

where $C = \frac{\pi r^2}{\rho c^2}$ is called the vessel compliance, and c is the pulse wave velocity. The limit of a rigid vessel is obtained when the vessel compliance vanishes, that is, when $C \rightarrow 0$.

Combining Eqs. 1 and 3 one obtains a harmonic oscillator equation for the pressure in frequency domain, namely,

$$\frac{\partial^2 \hat{p}}{\partial z^2} = -\kappa^2 \hat{p}, \quad (4)$$

where $\kappa^2 = \frac{i\omega C}{AK(\omega)}$.

Solving Eq. 4 for a single vessel, of length l , with known \hat{p}_{in} and \hat{p}_{out} for the inlet and outlet pressures on the vessel extremes, respectively, yields an analytical expression for the pressure along the vessel in frequency domain given by

$$\hat{p}(z) = \hat{p}_{in} \cos(\kappa z) + \frac{\hat{p}_{out} - \hat{p}_{in} \cos(\kappa l)}{\sin(\kappa l)} \sin(\kappa z), \quad (5)$$

which, when substituted in Eq. 1, provides the flow along the vessel in frequency domain,

$$\hat{q}(z) = M \left(\hat{p}_{in} \sin(\kappa z) - \frac{\hat{p}_{out} - \hat{p}_{in} \cos(\kappa l)}{\sin(\kappa l)} \cos(\kappa z) \right), \quad (6)$$

where $M^2 = i\omega C AK(\omega)$, for values of z in the interval $[0, l]$.

Blood rheology

The quantity $\hat{g}(\omega)$ appearing in the term β , defined after Eq. 2, is commonly known in the literature as *complex viscosity* η^* . It is the fourier transform of the complex relaxation modulus, introduced in the relation between the stress tensor and the rate-of-deformation tensor (see Eq. (4) in the Supplementary Material). It can be defined through a theoretical function in terms of frequency ω , shear viscosity η_0 , and one or several relaxation times, that describes the material rheology. It can also be obtained experimentally since it is related to the experimentally measured dynamic moduli $G'(\omega)$ and $G''(\omega)$ ^{26,27} through

$$\eta^*(\omega) = \hat{g}(\omega) = \frac{G''(\omega)}{\omega} + i \frac{G'(\omega)}{\omega}. \quad (7)$$

The dynamic elastic and viscous moduli, $G'(\omega)$ and $G''(\omega)$, respectively, characterize the response of a fluid to external forces. We have obtained the experimental rheology of human blood measured by passive microrheology within the viscoelastic linear regime at 27°C from the literature²⁸. The experimental values are discrete, so it is necessary to define fit functions to include them in a theoretical model. Here we chose simple quadratic fits for the log-log plot of the dynamic moduli, $G'(\omega)$ and $G''(\omega)$, vs ω . This is shown in Fig. 2. From these functions, we construct with Eq. 7, the blood complex viscosity, \hat{g} .

The step by step procedure to use experimental data of blood rheology into our model consist of: 1.- obtaining $G'(\omega)$ and $G''(\omega)$ from blood rheological experiments; 2.- fit experimental data with a chosen function in order to have continuous values for any ω ; 3.- obtain $\hat{g}(\omega)$ by means of Eq. 7; 4.- construct the auxiliary variable

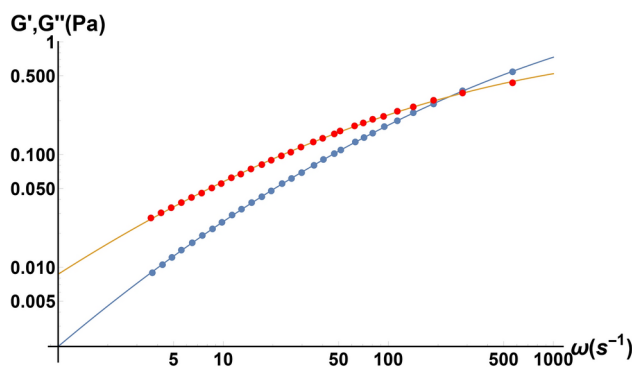


Fig. 2. Rheology of human blood measured by passive microrheology within the viscoelastic linear regime. Dots: elastic (blue) and viscous (red) moduli data digitalized from Fig. 1 of reference²⁸. Continuous lines: fits to the experimental data.

β , defined after Eq. 2; 5.- use β in the arguments of the Bessel functions in Eq. 2 in order to construct the permeability, which in turn enters the expressions for κ and M in Eqs. 5 and 6.

While it would be desirable to incorporate the blood rheology of each of the mammal species studied, this information is not known for most species, so we base the present model on the experimental blood rheology of humans, which has been best studied, and that, with the present study, it is now incorporated into our in-house GDEM, as described in the previous paragraph.

Flow through a network of vessels and network response

We use our in-house Generalized Darcy's Elastic Model (GDEM), developed and validated to describe the human arterial system²² and previously used to study the cooperation between elasticity and bifurcations in symmetric tree-like networks¹⁵. For symmetric tree-like networks (in which vessels bifurcate into identical vessels) we were able to relate linearly the velocity and the pressure gradient in frequency domain, in such a way that a dynamic response function could be written. The behavior of such response function can be translated in a straightforward manner to how a particular frequency of the pressure gradient affects flow.

As details of GDEM have been published elsewhere²², we limit the model description to the physical considerations it involves. Flow and pressure in each vessel conforming the network obey Eqs. 1 and 3. A node is defined as a point of bifurcation. Flow conservation is imposed at the nodes and pressures at extremes of vessels connected to a node are considered equal.

For instance, for a vessel at level k , with length l_k , that bifurcates into 2 vessels at level $k + 1$, with lengths l_{k+1} , flow conservation at the node joining these three vessels, implies an equation involving pressures at four points, namely, pressure at the node and (three) pressures at the opposite extremes of the vessels forming the node. For instance, flow conservation implies that output flow at level k , $\hat{q}_k(z = l_k)$ is equal to twice the input flow at level $k + 1$, $\hat{q}_{k+1}(z = 0)$, that is, $\hat{q}_k(z = l_k) = 2\hat{q}_{k+1}(z = 0)$. By using Eq. 6 in the equation for flow conservation at the node, we can write an equation relating the inlet pressure of the vessel at level k , the outer pressures of the two vessels at level $k + 1$ and the pressure at the node. For a node internal to the network, none of these pressures are known and must be determined as part of the solution. When one considers these arguments for each vessel in the network, the result is a system of equations for pressures at the network nodes, that can be solved, analytically or numerically, using the methodology described in the literature^{15,22}. Clearly, for nodes at the first and last level of the network, boundary conditions for pressure (or flow) must be specified. Once the pressure at the nodes is known, pressure and flow as a function of the position, z , along any vessel of the network, can be obtained by making use of Eqs. 5 and 6.

Flow along the vessels of an elastic network is clearly dependent on flow direction, so in order to have an integrated response for our system, we define a global response function (GRF), that would give information on flow spatially averaged along the flow direction, $\langle \hat{Q} \rangle_z(t)$. A GRF, χ_{global} , for a tree-like symmetric elastic network has been defined, in frequency domain, as²⁹

$$\chi_{global} = -\frac{L \langle \hat{Q} \rangle_z}{\Delta \hat{p}}, \quad (8)$$

where

$$\langle \hat{Q} \rangle_z = \frac{1}{L} \sum_{k=1}^N 2^{k-1} l_k \langle \hat{q}_k \rangle_z \quad (9)$$

Here, L is the total network length from the inlet to the outlet, $L = \sum_{k=1}^N l_k$, \hat{q}_k is the flow at position z in one of the vessels at level k , $\langle \hat{q}_k \rangle_z$ is the average flow along a single vessel at level k and $2^{k-1} \langle \hat{q}_k \rangle_z$ is the total flow at level k .

Geometric network for humans and considerations for other mammals

We study the pulsatile flow of blood confined in a tree-like arterial network whose bifurcating structure follows different rules depending on whether the bifurcating vessel is a large or a small artery. Large arteries bifurcate according to an area preserving law for radii

$$r_k = \left(\frac{1}{2}\right)^{\frac{k-1}{2}} r_{aorta}, \quad (10)$$

while small arteries bifurcate according to Murray's law¹

$$r_k = \left(\frac{1}{2}\right)^{\frac{k-k^*}{3}} r_{k^*}. \quad (11)$$

The two regions of the network, separated by a crossover level k^* , have lengths that also follow different exponents depending on whether they are large or small arteries, where large and small refer to radii, not to lengths.

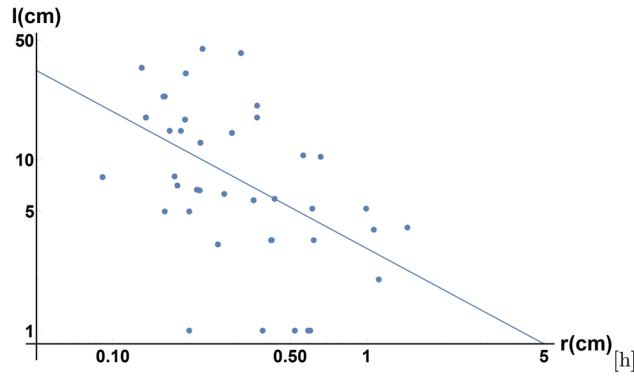


Fig. 3. Lengths as a function of radii for large human arteries. Continuous line: fit to the observed data, $l = 3.04 r^{-0.80}$, with l and r measured in cm. Data adapted from Table 1 in reference²³.

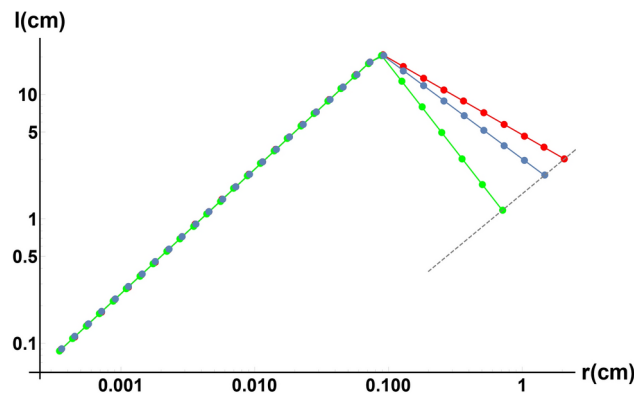


Fig. 4. Vessel length as a function of radius in the arterial network of different mammals. At small radii, length is proportional to radius and independent of the species weight, according to Eq. 13. For arteries of large radius, the blue curve indicates the slope obtained from data of large arteries in humans in Fig. 3. The green curve corresponds to mammals of $W = 40$ kg (a dog, for instance) and the red curve to a mammal of $W = 600$ kg (a cow, for example). The dotted line on the right hand side of the plot, corresponds to the relation between length and radius for the aorta, given by $l_{aorta} = 1.59 r_{aorta}^{0.89}$.

For large human arteries, lengths as a function of average radius have been taken from a 55-vessel model of the arterial system that describes with good accuracy the human arterial tree²³. We have characterized the length versus radius dependance with a power law exponent, $l = 3.04 r^{-0.80}$, with l and r measured in cm. The fit was done with a simple linear regression of the logarithm of length data and the logarithm of radius data. Notably, in this region of the tree, as a general trend, length increases as radius decreases, reflecting the characteristics illustrated properly by the cases of the ascending aorta (with large radius and small length) and the femoral arteries (with smaller radii and larger lengths), see Fig. 3.

For small arteries on the other hand (like arterioles and capillaries), a space filling hypothesis¹ together with Murray’s law for radii, dictate that length increases linearly as a function of radius. That is, the space filling hypothesis implies that lengths follow

$$l_k = \left(\frac{1}{2}\right)^{\frac{k-k^*}{3}} l_{k^*} , \tag{12}$$

which, together with Eq. 11, imply that

$$l_k = \frac{l_{k^*}}{r_{k^*}} r_k = \frac{l_{capillaries}}{r_{capillaries}} r_k . \tag{13}$$

Continuity of the curve length vs radius determines the crossover level k^* separating the two regimes. This one corresponds to the blue dot with maximum length in Fig. 4.

For other species, we consider that the number of levels for small arteries is constant across species¹ so that the curve of length as a function of radius in this range does not depend on body mass. That is, for small arteries, the linear relation between length and radius is preserved across species. Finally, we use documented data in the literature from mice to horses, to know how the length and radius of the aorta are related to each other. These ones, do not decrease (increase) in a proportional way, but with an exponent slightly smaller than one, namely, $l_{aorta} \sim r_{aorta}^{0.89}$. Continuity of the curve length vs radius determines the slope for large arteries, for species other than human. The network construction is illustrated in Fig. 4 for three mammals.

Radii of vessels is strongly correlated with vessel elasticity. For the human arterial tree, the pulse wave velocity, c , is given by the empirical relationship $c = \frac{13.3}{(2r)^{0.3}}$ (in m/s), with r measured in millimetres³⁰. That is, the smaller the radii, the larger the pulse wave velocity, the stiffer the vessel and the smaller the compliance in Eq. 3. This empirical relationship is particularly good for large arteries³⁰, but due to lack of experimental information, we will consider it valid all along the arterial tree. Also, for other mammal species we consider the same relationship known for humans.

Results

In Fig. 5, we plot the modulus of the response function (Eq. 8) as a function of frequency for the networks of the three mammals whose geometry is represented in Fig. 4. We observe that the curves have maxima: for a given curve, the first maximum corresponds to the largest response (the lowest resistance to flow), and the frequency at which the first maximum occurs decreases with increasing mammal size.

We collect the resonance frequencies as a function of the arterial radius, report them in Table 1, and plot them in Fig. 6. The continuous red line is the slope obtained from a fit to model data, indicated with red dots, giving a scaling law of the form $\nu_{resonance} = (3.27 \pm 0.06)r_{aorta}^{-0.45 \pm 0.02}$. When comparing with our reference curve given by the best fit to the purple dots in Fig. 6 $\nu_{heart} = (1.25 \pm 0.05)r_{aorta}^{-0.43 \pm 0.05}$, and indicated with a continuous purple line, we find that there is an excellent agreement for the slope, within error bars. That means that our model correctly captures the rate at which heart rate changes with aorta radius across species in the range of 1 to 3800kg, corresponding to mammals ranging from ferrets to African elephants. However, it is clear that model frequencies are above the observed ones by a factor of approximately 2.6.

Discussion

Figure 6 demonstrates excellent agreement between the model (red line) and the observed (purple line) scaling exponents for frequency as a function of aorta size. This supports our hypothesis that the frequency maximizing the dynamic response -while minimizing resistance to flow- determines the heart rate, which governs blood flow in the arterial system.

While our model accurately captures the rate of change of frequency as a function of aorta radius across species for animals with masses ranging from 1 to 3800 kg, it exhibits a clear limitation: the predicted frequencies are approximately 2.6 times higher than observed values for the heart rates. Future studies could address this discrepancy by exploring alternative models for vessel elasticity in small vessels, as vessel radii are strongly correlated with elasticity. In this work, we have adopted an empirical relation, derived from large human arteries, to model pulse wave velocity as a function of radius, which is good for vessels above 2.5 mm³⁰. However, due to the lack of experimental data, we assumed this relation to hold throughout the entire arterial tree.

The idea that the frequency that maximizes the dynamic response between flow and pressure gradient in frequency domain, and eases fluid movement, coincides with a physiological frequency, was proposed as a plausible explanation for heart rates in mammals over a decade ago². In this work, we have revisited the original project to review all the considerations made in the model. Substantial changes have been included: 1.- we have considered the experimental rheology of human blood instead of considering blood as a Maxwell fluid; 2.- we have considered elastic networks instead of rigid ones; 3.- we have considered a completely different structure for the geometry of large arteries and the geometry of small ones, both, in the way radii and lengths

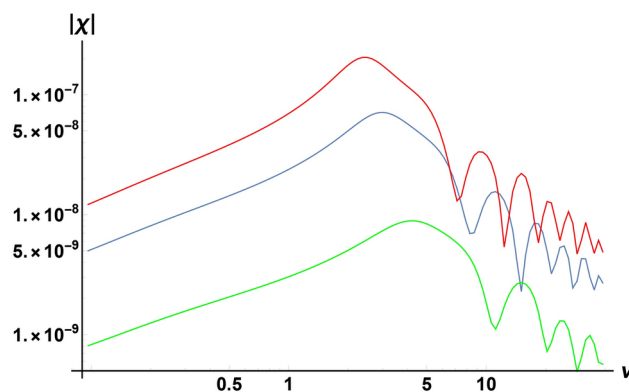


Fig. 5. Response of the arterial networks for three mammals corresponding to: humans (blue curve), dog (green curve) and cow (red curve). The position of the first maximum indicates how the resonance frequency varies as a function of system size.

r_{aorta} (cm)	Number of large arterial levels	$\nu_{resonance}$ (Hz)
4.00	12	1.51
3.50	12	1.67
3.00	11	1.94
2.50	11	2.14
2.00	10	2.49
1.74	10	2.61
1.47	9	3.04
1.24	9	3.04
1.00	8	3.71
0.85	8	3.71
0.70	7	4.32
0.60	7	4.10
0.50	6	4.77
0.40	6	5.01
0.30	5	5.27
0.27	5	5.54
0.25	4	5.82
0.20	4	6.12

Table 1. Model results for the resonance frequency that maximizes the dynamic response. On the first column we have radius of aorta, ranging from 0.20 cm to 4.0 cm. On the second column, we find the number of bifurcating levels in the model for large arteries, as illustrated in Fig. 4 for 3 species. On the third column, we have the resonance frequency of the dynamic response function.

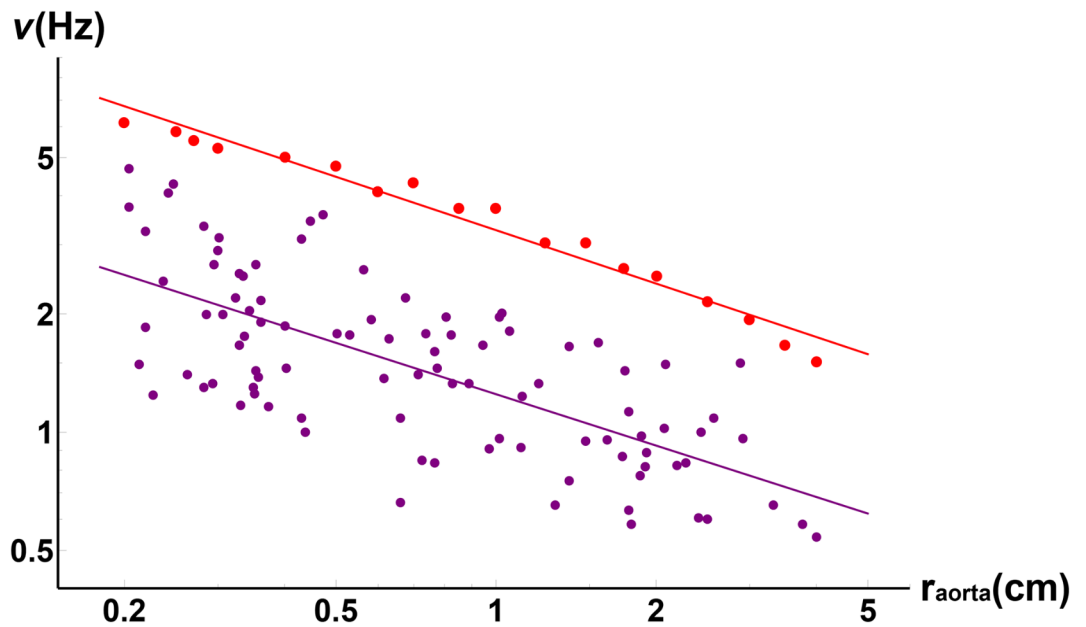


Fig. 6. Large red dots are model results for the resonance frequency, that maximizes the dynamic response, vs the radius of aorta from 0.20 cm to 4.0 cm (data are on table of Fig. 1). The continuous red line is the slope obtained from a fit to this data, giving a scaling of the form $\nu_{resonance} = 3.27r_{aorta}^{-0.45}$. Purple dots are the heart rates for mammals of Fig. 1, in terms of aorta radius by means of the transformation $r_{aorta} = 0.21W^{0.36}$, obtained from Holt²⁴. The continuous purple line, is the best fit to these data, giving a scaling of the form $\nu = 1.25r_{aorta}^{-0.43}$ which we take as a reference curve. Both continuous lines in the figure were obtained with a simple linear regression of the logarithm of frequency data and the logarithm of aorta radius data.

progress with bifurcation level according to observational information in the literature; 4.- for validation, we have taken observed data of heart rate vs body mass for 95 mammals and used a scaling relation for the aorta radius as a function of body mass from the literature²⁴, that allowed us to have heart rate data as a function of aorta radius, that follow a scaling law given by $\nu = 1.25r_{aorta}^{-0.43}$. These changes have allowed us to predict

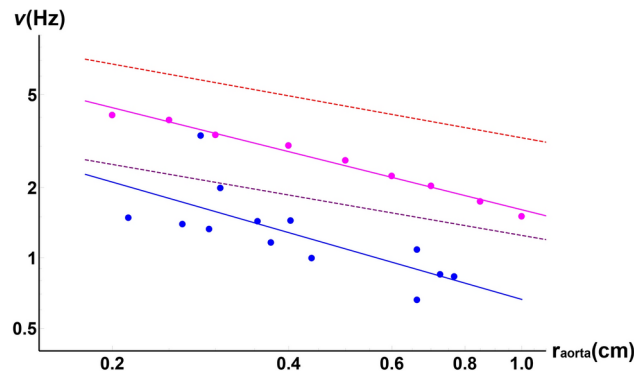


Fig. 7. Blue dots are the heart rates for marsupials, of the proper subgroup of points of Fig. 1, in terms of aorta radius by means of the transformation $r_{aorta} = 0.21W^{0.36}$, obtained from Holt²⁴. The continuous blue line, is the best fit to these data, giving a scaling of the form $\nu_{heart} = 0.65 r_{aorta}^{-0.77}$. Magenta dots are model results for the resonance frequency, that maximizes the dynamic response, vs the radius of aorta for an arterial system with a much larger elasticity than the one used in Fig. 6 (a pulse wave velocity equal to one quarter of the value previously used). The continuous magenta line is the slope obtained from a fit to these data, giving a scaling of the form $\nu_{resonance} = 1.61 r_{aorta}^{-0.63}$. With dotted lines we have indicated, for reference, the purple and red lines of Fig. 6. We can observe that a more elastic network produces an effect in resonance frequency consistent with changes observed in marsupials, when compared with the larger group of mammals. That is, the difference between the dotted red line and the continuous magenta line is qualitatively similar to the difference between the dotted purple line and the continuous blue line. That is, the frequency value decreases while the value of the magnitude of the slope slightly increases.

$\nu_{resonance} = 3.27 r_{aorta}^{-0.45}$ for the frequency that maximizes the dynamic response and minimizes resistance to flow, with a continuum mechanical model.

To reconnect our results with observed data, collected as a function of body size, we note that our model proposes that what determines resting heart rates in mammals is the rate at which blood flows with the least possible resistance through the whole arterial network. To show that, we have chosen the aorta radius as one of the possible characteristic scales of the arterial system. Our model says that the rate at which blood flows depends largely on the size of the arterial system, which in turn scales positively with body size. Such positive relationship between arterial system size and body size may then explain why animals with larger bodies tend to have lower resting heart rates, though there is still a substantial amount of variation among species that might be due to particular anatomical details, as well as particularities of blood composition and vessel elasticity adapted to particular environments.

While our research has focused on understanding a fundamental feature of the evolution and physics of resting heart rates, our model also suggests a way forward toward understanding heart rates or the arterial systems of particular groups of mammals. For instance, marsupials tend to have a lower basal metabolic rate (BMR) compared to placental mammals of similar size. This lower BMR reflects their reduced energy requirements to sustain basic physiological functions and is associated with slower physiological rates, including heart rate³¹. This can be observed for the 13 observed marsupial heart rates among our group of 95 mammals. See blue dots and continuous blue line in Fig. 7. For reference a purple dotted line indicates the corresponding quantity for the group of 95 mammals of Fig. 6. In the figure we can observe not only that marsupials have considerably lower heart rates than the larger group, but that the magnitude of the slope of heart rate versus aorta radii increases with respect to the one of the 95 mammals' group (compare the slope of the continuous blue line and the one of the purple dotted lines). Our model predicts that a much more flexible arterial system - a pulse wave velocity equal to one quarter of the value used in the reference model - would give resonance frequencies that are considerably smaller than the ones of the group of 95 mammals. See pink dots and continuous pink line in Fig. 7. For reference a red dotted line indicates the corresponding quantity for the group of 95 mammals of Fig. 6. Moreover, a more flexible arterial system gives a qualitative change in slope comparable to the one of the observational data for marsupials, that is the magnitude of the slope of the pink continuous line is larger than the one of the red dotted line. These observations can therefore be used as a departure point to test, for instance, if vessel elasticity in marsupials is much larger than the one of the rest of mammals, as our model suggests. This can be done by non-invasive techniques such as Pulse-Wave-Velocity, which is a well-established technique used to assess vessel elasticity.

Animal data are unavoidably affected by large uncertainties since heart rates are often measured on anaesthetized or restrained specimens³². When it comes to the inter-species variability - reflected in the heart rate of 95 mammals in Figs. 1 and 6 -, it is clear that the circumstances in which their heart rate was measured were different, since these measurements do not come from the same study but from several dozens studies. Also, it is worth remembering that evolution is an on-going process and that even though with several hundred million years of mammalian evolution processes tend to be optimized, different species have been successful in different degrees. Factors, such as habitat, contribute to such deviations. For instance, cold environments promote strategies that lower metabolic rates and reduce heart rates to conserve energy, whereas warmer conditions

require adjustments to prevent overheating³³. Also, animals living at high altitudes, in which a lower air oxygen content is available, often adjust their heart rates to conserve oxygen³⁴. In general heart rate varies with food availability, environmental conditions, and species-specific adaptations³⁵. In order to study a specific group of mammals with our model, the experimental blood rheology, experimental vessel elasticity and observational morphological network description, representative of that particular group, would be required.

Our model also suggests a way forward towards practical applications within individual species. For example, within model organisms, veterinary animals or humans, one might explore the ways in which clinical changes in heart rate or vasculature lead to mismatches between actual and ideal heart rates. For example, for animals of few tens of kilograms, our model predicts that when arteries become more rigid, resonance frequencies become larger, possibly correlating with larger heart rates.

The coupling between blood viscoelasticity and vessel elasticity considered in our model is crucial in determining the power law dependence of the resonance frequency as a function of the aorta radius. When considering blood as a simple Newtonian fluid, our model predicts a power law with a much smaller exponent, 0.27, instead of the one of 0.45 depicted in Fig. 6.

Clearly, we do not intend to simulate precisely blood flow in particular vessels. For instance, blood flow in capillaries whose sizes are comparable to red blood cells (which are less than 10μ), might need an approach different from a continuum one. But since vessel sizes in the arterial systems of mammals span for over 3.5 decades (see Fig. 4), and the continuum approach might be considered a reasonable approximation for vessels over 30μ in radius, we can say that a continuum mechanics approach, such as ours, is modeling correctly slightly under 3 decades in radii. Moreover, we have checked that if we leave out the smallest capillaries from our model, and leave only vessels with over 30μ in radius, results for the frequency that maximizes the response function do not change.

It is worth noting that flow in the human arterial system (with a non-symmetric geometry) can be accurately described with our methodology, which has proven to be as good as fully non-linear 3-dimensional simulations to describe blood and pressure flow waves in the large arteries of the arterial system²². However, if one wished to break the geometrical symmetry of the present tree-like model, it would not be possible to write down a scalar response function as for the symmetric network. In that case, a tensor response function could be written to describe the response between any two inlet/outlet points in the network. Alternatively, a path from the aortic inlet to a distal artery can be used to define a scalar response function. To assess how the symmetry of the network affects the frequency at which the response function reaches its maximum, we modeled the 20-vessel asymmetric human arterial network studied in reference²². We selected a path extending from the aortic entrance to the end of the left iliac artery. By analyzing the dynamic response as a function of frequency (not shown), we determined that the maximum occurs at 2.4Hz, similarly far from the actual human heart rate (approximately 1.2Hz) as the prediction of the symmetric network. This suggests that asymmetry is not the aspect where the model could be most improved. Instead, the hypothesis of a different scaling law for the elasticity of small vessels remains the most promising avenue for future work.

Data availability

All data generated or analysed during this study are included in this published article and its supplementary information files.

Received: 29 April 2024; Accepted: 17 February 2025

Published online: 27 February 2025

References

- West, G. B., Brown, J. H. & Enquist, B. J. A general model for the origin of allometric scaling laws in biology. *Science* **276**, 122 (1997).
- Flores, J., Corvera Poiré, E., del Río, J.-A. & López de Haro, M. A plausible explanation for heart rates in mammals. *J. Theor. Biol.* **265**, 599–603 (2010).
- Clerk Maxwell, J. On the Dynamical Theory of Gases. *Philos. Trans. R. Soc. Lond.* **157**(20), 49–88 (1867).
- Zhou, M.-Y. & Sheng, P. First-principles calculations of dynamic permeability in porous media. *Phys. Rev. B* **39**, 12027 (1989).
- López de Haro, M., del Río, J.-A. & Whitaker, S. Flow of Maxwell Fluids in Porous Media. *Transp. Porous Media.* **25**, 167–192 (1996).
- del Río, J.-A., López de Haro, M. & Whitaker, S. Enhancement in the dynamic response of a viscoelastic fluid flowing in a tube. *Phys. Rev. E* **58**, 6323. (1998); Erratum *Phys. Rev. E* **64**, 039901 (2001).
- Tsiklauri, D. & Beresnev, I. Enhancement in the dynamic response of a viscoelastic fluid flowing through a longitudinally vibrating tube. *Phys. Rev. E* **63**, 046304 (2001).
- Cuevas, S. & del Río, J.-A. Dynamic permeability of electrically conducting fluids under magnetic fields in annular ducts. *Phys. Rev. E* **64**, 016313 (2001).
- Collepardo-Guevara, R. & Corvera Poiré, E. Controlling viscoelastic flow by tuning frequency during occlusions. *Phys. Rev. E* **76**, 026301 (2007).
- Castro, M., Bravo-Gutiérrez, M.-E., Hernández-Machado, A. & Corvera Poiré, E. Dynamic characterization of permeabilities and flows in microchannels. *Phys. Rev. Lett.* **101**, 224501 (2008).
- Corvera Poiré, E. & Hernández-Machado, A. Frequency-induced stratification in viscoelastic microfluidics. *Langmuir* **26**, 15084 (2010).
- Bravo-Gutiérrez, M.-E., Castro, M., Hernández-Machado, A. & Corvera Poiré, E. Controlling viscoelastic flow in microchannels with slip. *Langmuir* **27**, 2075 (2011).
- de la Guerra Pablo, A. & Corvera Poiré, E. Pulsatile parallel flow of air and a viscoelastic fluid with multiple characteristic times. An application to mucus in the trachea and the frequency of cough. *J. Phys.: Condens. Matter* **34**, 314003 (2022).
- Torres Rojas, A.-M., Pagonabarraga, I. & Corvera Poiré, E. Resonances of Newtonian fluids in elastomeric microtubes. *Phys. Fluids* **29**, 122003 (2017).
- Yáñez, D., Travasso, R. D. M. & Corvera Poiré, E. Resonances in the response of fluidic networks inherent to the cooperation between elasticity and bifurcations. *R. Soc. Open Sci.* **6**, 190661 (2019).

16. Torres Rojas, A.-M. & Corvera Poiré, E. Cooperation and competition of viscoelastic fluids and elastomeric microtubes subject to pulsatile forcing. *Phys. Rev. Fluids* **5**, 063303 (2020).
17. Lombard, J., Pagonabarraga, I. & Corvera Poiré, E. Dynamic permeability of a compressible binary fluid mixture. *Phys. Rev. Fluids* **5**, 064201 (2020).
18. Castrejón-Pita, J.-R., del Río, J.-A., Castrejón-Pita, A.-A. & Huelsz, G. Experimental observation of dramatic differences in the dynamic response of Newtonian and Maxwellian fluids. *Phys. Rev. E* **68**, 046301 (2003).
19. Torralba, M. et al. Measurements of the bulk and interfacial velocity profiles in oscillating Newtonian and Maxwellian fluids. *Phys. Rev. E* **72**, 016308 (2005).
20. Vázquez-Vergara, P., Torres-Herrera, U., Olguin, L.-F. & Corvera Poiré, E. Singular behavior of microfluidic pulsatile flow due to dynamic curving of air-fluid interfaces. *Phys. Rev. Fluids* **6**, 024003 (2021).
21. Vázquez-Vergara, P., Torres-Herrera, U., Caballero-Robledo, G.-A., Olguin, L.-F. & Corvera Poiré, E. Experimental resonances in viscoelastic microfluidics. *Front. Phys.* **9**, 636070 (2021).
22. Flores, J., Alastruey, J. & Corvera Poiré, E. A novel analytical approach to pulsatile blood flow in the arterial network, *Ann. Biomed. Eng.* **44**, 3047–3068 (2016).
23. Stergiopoulos, N., Young, D. F. & Rogge, T. R. Computer simulation of arterial flow with applications to arterial and aortic stenoses. *J. Biomech.* **25**, 1477–1488 (1992).
24. Holt, J. P., Rhode, E. A., Holt, W. W. & Kines, H. Geometric similarity of aorta, venae cavae, and certain of their branches in mammals. *Amer. J. Physiol.-Reg. Integrat. Comp. Physiol.* **241**, R100–R104 (1981).
25. Zhang, G. Q. & Zhang, W. Heart rate, lifespan, and mortality risk. *Age. Res. Rev.* **8**, 52–60 (2009).
26. Bird, R. B., Stewart, W. E. & Lightfoot, E. N. *Transport phenomena* (Wiley, 2006).
27. Tschoegl, N.-W. *The phenomenological theory of linear viscoelastic behavior: An introduction* (Springer, 2012).
28. Campo-Deaño, L., Dullens, R. P. A., Aarts, D. G. A., Pinho, F. T. & Oliveira, M. S. N. Viscoelasticity of blood and viscoelastic blood analogues for use in polydimethylsiloxane in vitro models of the circulatory system. *Biomacromolecules* **7**, 034102 (2013).
29. González Mena, L. Flow in elastic networks subject to pulsatile forcing, Treball de Fi de Màster. Universitat de Barcelona (2016). <https://diposit.ub.edu/dspace/handle/2445/103675>
30. Circ, Heart et al. Validation of a one-dimensional model of the systemic arterial tree. *Am. J. Physiol. Physiol.* **297**, H208–H222 (2009).
31. McNab, B. K. The comparative energetics of placental and marsupial mammals. *J. Comp. Physiol. B.* **178**, 877–892 (2008).
32. Verzicco, R. Electro-fluid-mechanics of the heart. *J. Fluid Mech.* **941**, P1 (2022).
33. Tattersall, G. J. et al. Coping with thermal challenges: Physiological adaptations to environmental temperatures. *Compr. Physiol.* **2**, 2151–2202 (2012).
34. Arieli, R. & Ar, A. Heart rate responses of the mole rat (*Spalax ehrenbergi*) in hypercapnic, hypoxic, and cold conditions. *Physiol. Zool.* **54**, 14–21 (1981).
35. McNab, B. K. *The physiological ecology of vertebrates: a view from energetics*. Cornell University Press (2002).

Acknowledgements

The authors thank Aimee M. Torres Rojas and Diana Yañez Guarneros for permitting us to reference their unpublished results on the frequency that maximizes the response function in a model of an asymmetric human arterial network. RT thanks the support of FEDER funds through the Operational Programme Competitiveness Factors, COMPETE, and Fundação para a Ciência e a Tecnologia through the strategic projects UIDB/04564/2020 and UIDP/04564/2020 with DOI identifiers 10.54499/UIDB/04564/2020 and 10.54499/UIDP/04564/2020, respectively. ECP acknowledges financial support from the Faculty of Chemistry, UNAM, through PAIP program 5000-9011 and from DGAPA, UNAM, through PAPIIT Project IN113421.

Author contributions

ECP conceptualized the project. RDMT and ECP developed the model, carried out the calculations, the data curation and formal analysis, and wrote the first draft of the manuscript. CAP collected observed mammal data from the literature. All authors discussed the results and limits of the model and review and edited the final version of the manuscript.

Declarations

Competing interests

The authors declare no competing interests.

Additional information

Supplementary Information The online version contains supplementary material available at <https://doi.org/10.1038/s41598-025-90928-x>.

Correspondence and requests for materials should be addressed to E.C.P.

Reprints and permissions information is available at www.nature.com/reprints.

Publisher's note Springer Nature remains neutral with regard to jurisdictional claims in published maps and institutional affiliations.

Open Access This article is licensed under a Creative Commons Attribution-NonCommercial-NoDerivatives 4.0 International License, which permits any non-commercial use, sharing, distribution and reproduction in any medium or format, as long as you give appropriate credit to the original author(s) and the source, provide a link to the Creative Commons licence, and indicate if you modified the licensed material. You do not have permission under this licence to share adapted material derived from this article or parts of it. The images or other third party material in this article are included in the article's Creative Commons licence, unless indicated otherwise in a credit line to the material. If material is not included in the article's Creative Commons licence and your intended use is not permitted by statutory regulation or exceeds the permitted use, you will need to obtain permission directly from the copyright holder. To view a copy of this licence, visit <http://creativecommons.org/licenses/by-nc-nd/4.0/>.

© The Author(s) 2025